PREDICTION OF UNSTEADY FLOWS AROUND ROTATING BLADES

Jean-Marc Bousquet
ONERA, Applied Aerodynamic Department
92322 Chatillon France

Keywords: *Helicopter, Propeller, Turbomachinery, Unsteady Flows, Euler, Navier-Stokes*

Abstract

This paper presents a review of 3D unsteady Euler and Navier-Stokes computations performed at ONERA with the CANARI code and more recently with the elsA software around rotating devices as propeller blades, helicopter rotor blades and turbomachinery bladings. Validation of the unsteady computations is made by comparison with experimental data.

1. Introduction

The on-going progress in computational resources along with the improvement of the numerical methods make it possible to simulate the 3D time-accurate flow field around the rotating parts of the aircraft as the helicopter rotor, the turboprop or a turbomachinery blade in a multi-stage turbofan engine. For these complex applications, the methods need to be efficient and accurate. Although a considerable effort has been paid for years at ONERA to validate CFD codes for steady applications, it is clear that a significant effort has to be carried on for the validation of the unsteady computations by comparison with experimental data.

This paper presents a review of different 3D unsteady computations performed at ONERA with the CANARI code and more recently with the *elsA* software around rotating devices as propeller blades[1], helicopter rotor blades [2] and turbomachinery bladings[3].

After a brief description of the methods, typical unsteady flow applications will be successively presented on propellers in incidence or in interaction, on helicopter rotors where the blade deformation has to be accounted for and on turbomachinery bladings where viscous effects are of prime importance in the flow development.

2. Computation methods

The basic numerical method is the CANARI code [5][6], which is currently moved into the more general *elsA* software. This is a general Euler and Navier-Stokes solver on multi-block structured grids, which uses an implicit finite volume scheme with a multi-step time technique. The explicit stage is a 4-step Runge-Kutta space-centered type scheme as proposed by Jameson. Second and fourth order dissipation terms are added in order to capture flow discontinuities. The implicit stage is the Implicit Residual Smoothing [4].

The CANARI unsteady solver was first used for turbomachinery applications[14], with the equations discretized in the relative rotating frame in a " cell-vertex " approach ; for propeller applications, a "cell-centered" scheme is used. Typical physical boundary treatments are based on the characteristic relations.

Helicopter functionalities, originally implemented in the WAVES Euler code[10] have been recently moved into the *elsA* software[11][2]. In particular, the Arbitrary Lagrangian Eulerian formulation (ALE) allows to solve the Euler or Navier-Stokes equations on a moving grid which accounts for the displacement of the articulated and deforming rotor blades. The blade motion is defined by an harmonic decomposition of the blade rotation angles around the pitch, flap and lag hinges, while blade deformations are given in a modal

form as a result of a separate aeroelastic computation with the HOST code [12].

3. Propeller

The flow unsteadiness appears on a rotating blade as soon as the rotation axis is not aligned with the upstream flow velocity, which is the case of a propeller at incidence.

Based on the ONERA experience on high speed propellers[7], the validation is made on the APIAN propeller (figure 1), at the upstream Mach number M=0.7, advance ratio J=3.12 and blade angle β=57° with an incidence angle α=3°, as in the ONERA/S1MA wind tunnel test[8][9]. For this case with no flow symmetry or periodicity, the computation domain includes the 6 inter-blades channels in a multiblock strategy. In total, about 2 million grid points are used. The Euler computation is initialised with a steady solution at M=0.7 with an incidence α=0°. Then, the unsteady computation is run until a periodic solution is obtained (after about 3 complete propeller revolutions).

Figure 2 shows the instantaneous pressure coefficient distribution on the blade at r/R=0.75. A clear asymmetry is seen which follows the airfoil local inflow angle of attack evolution : larger local angle of attack on the down-going blade side (ψ=90°) than on the up-going blade side (ψ=270°). The general good agreement with experimental results validates the unsteady approach.

Integration of the blade aerodynamic loads provides strong periodic fluctuations on the propeller forces projected in the absolute reference frame (figures 3 and 4). While the thrust coefficient evolution is nearly sinusoidal as function of the azimuth ψ (figure 3), the lateral force coefficient evolution (figure 4) is clearly more complex. For analysing these phenomena, an additional computation was run at M=0.3, where the flow is no more transonic on the blades. Figure 3 shows no strong modification of the thrust fluctuation which stays nearly sinusoidal. On the other hand, figure 4 shows important differences on the lateral force computed at M=0.7 and M=0.3. As a general trend, the M=0.3 evolutions are nearly sinusoidal, with significant phase shifts from M=0.7 solution in the azimuth of maximum lateral force.

This transonic effect is also visible on figure 5 where the lateral force coefficient is integrated over one revolution on the 6 blades. The computed lateral force coefficient has a linear evolution with the propeller incidence, while the test results indicate non-linearities for α>2°. The transonic effect is important, as the M=0.7 and M=0.3 Euler computation results differ by 100%. As the quasi-steady LPC method cannot detect any lateral force component, only the unsteady Euler computation result is of practical interest at M=0.7, with a computed lateral force coefficient which differ by less than 20% from the test result at α=3°.

Propeller/airframe interaction

The account of aerodynamic interaction has been validated on a generic configuration of a four-propeller transport aircraft provided by Airbus France.

During the test of a half-model of this generic configuration in the ONERA S1MA wind tunnel, different configurations have been evaluated, including the complete configuration with two propellers operating as represented on figure 6. For the validation exercise, a configuration with only the inboard propeller active has been selected.

The ICEM-CFD Hexa Software was used to construct the 3D structured grid with a continuous interface between the blocks rotating with the propeller and the fixed blocks around the aircraft. The complete 3D mesh is made of 109 blocks with about 2.9 10^6 nodes. The rotating domain containing the propeller and the spinner is made of 21 blocks, with about 3.5 10^5 nodes.

The numerical application was performed with the aerodynamic flow conditions of the S1MA wind tunnel test at M=0.68. The propeller conditions have been set to J=3.51 and β=62° as in test. The half aircraft computation was converged after two propeller revolutions, when pressure coefficient evolutions on two successive blades were almost identical.

As an example, an instantaneous pressure distribution on the aircraft and on the propeller is given on figure 7. One can notice the asymmetry of the flow development on the different blades which illustrates the unsteadiness of the flow characteristics on each blade. This is confirmed on figures 8 and 9 where the integration of the aerodynamic force on one blade is plotted as a function of time (time is referenced by the ψ azimuth of the blade). In the axial direction, the thrust component of the blade force (figure 8) has a nearly sinusoidal evolution which is similar to the thrust coefficient evolution on the same isolated propeller computed at M=0.68 and α=3°.

On the lateral force component, figure 9 shows that the interaction has a significant influence on the propeller force which differ from the isolated propeller computation in the 120°<ψ<240° zone. In this case, the installation effect does not only change the modulus but also the sign of the lateral force coefficient on the propeller, when integrating the lateral force component over a propeller revolution.

On the aircraft wing and nacelle, analysis of the interaction shows that the computed instantaneous pressure distribution is in a general good agreement with experiment [1].

The unsteady influence of the propeller flowfield on the aircraft is analysed on figures 10 and 11. On these figures, one has plotted the difference of the flow solutions computed at ψ=0° and ψ=30° ; for this 6 bladed propeller, the $\Delta\psi$=30° time difference corresponds to half the period of a blade passage in front of a fixed position on the wing. On the wing upper side (figure 10), one clearly sees the helicoidal trace of blade wakes on the nacelle, which are zones of reduced Mach number. Figure 10 shows also significant unsteady effects on the inner part of the wing, mostly in the zone immersed in the propeller slipstream, with an oblique progression of the higher and lower Mach number zones, which illustrates the axial progression of the blade wakes interactions on the wing. On the wing lower side (figure 11), similar phenomena are noticed, with traces of the blade roots wakes on the nacelle close to the propeller, and traces of the wakes interaction on the inner part of the wing.

In summary, the influence of unsteady interaction is mostly located in the inner part of the wing which is a zone where the transonic effects are significant on such a transport aircraft.

4. Helicopter

On the helicopter rotor, the flow is naturally unsteady, as the rotation axis is nearly normal to the forward flight direction.

Figure 12 illustrates this phenomenon by mapping the relative Mach number contours around the four blades of the 7AD rotor. For the blade in the advancing side region (ψ=90°), the summation of rotation velocity and axial velocity results in transonic flows in the external parts of the blade, while low velocity levels are encountered on the blade in the retreating side region (ψ=270°). This periodic evolution of the flow characteristics is amplified by the rotor controls with cyclic changes of the blade angle of attack.

As part of the CHANCE program towards Complete Helicopter Computation, the validation of the 3D Euler solution is made by comparison with S1MA wind-tunnel results, on the highly instrumented four bladed 7A and 7AD rotors, which mainly differ by blade tip shape (figure 13). During these tests, the rotors were trimmed according to the "Modane law" (β_{1s}=0, β_{1c}= -θ_{1s}). The test cases selected for this study are defined by an advance ratio μ=0.4, a tip rotational Mach number $M_{\Omega R}$=0.646 and a fuselage drag coefficient CdS/Sσ=0.1. Several rotor lift coefficients Zb have been chosen, ranging from approximately 12.5 to 17.5.

As illustrated on figure 14, the addition of a swept tip on the 7AD blade reduces significantly the transonic effects in the tip region of the advancing blade at ψ=90°.

The unsteadiness of the flow is illustrated on figure 15 where one compares on the 7A rotor, contours of both computed and experimental sectional lift coefficients C_nM^2

obtained by integration of blade pressure distributions. In particular, one notices the non-symmetric aerodynamic loading on both sides of the ψ=90° line which indicates different flow development around the advancing blade, depending on the acceleration or the deceleration of the relative flow. In addition, figure 19 shows that an increase of the rotor lift Zb (from Zb=12.56 to Zb=14.8) is mostly located in the front (ψ=180°) and rear (ψ=0°) parts of the rotor disk. This trend is well predicted by the Euler computations. One also notices a phase lag in the position of the area of the computed minimum (negative) lift by comparison with experiment.

Blade deformation account

The grids generated for this study are made of one C-H block per blade. For treating the four bladed 7A rotor, the four blocks grid is made of 141x40x26=146.640 nodes, with a total of 586.560 points. Figures 16 and 17 illustrate the grid deformation technique included in the ALE strategy which propagates a deformation (strongly exaggerated on these figures) in the whole field surrounding the 7A blade. In this Euler computation, the time step corresponds to Δψ=0.1°. In such high speed conditions (μ=0.4), the solution becomes periodic after one rotor revolution.

Unsteady pressure distributions plotted on figure 18 confirm that the 3D Euler method predicts accurately the evolution of the blade aerodynamic loading for most of the blade rotation, with some differences mainly in the inner part (r/R=0.5) of the blade retreating side region (180°<ψ<360°) where flow separation occurs. In the blade tip region (r/R=0.975), the transonic flow development is sensitive to blade deformations, as illustrated on the advancing blade (ψ=90°) by the different shock waves locations due to blade elasticity account in the computation.

The influence of the blade deformations on the sectional lift coefficients C_nM^2 is illustrated on figure 19. The amplitude and phase of the peak of negative airloads for the most outboard sections (r/R=0.975) are better predicted by the soft blade computations as a result of torsion elastic deformations. Nevertheless, there are still differences with experiment on the advancing blade which require improved aeromechanic analysis.

In summary, the account of interaction between blade deformations and unsteady aerodynamic loads on blade tips [13], as well as the account of unsteady viscous phenomena on retreating blades, which are both under development, will be of prime interest for improving rotor computation in forward flight.

5. Turbine stage

The account of flow viscosity is essential for turbomachinery applications, requiring the use of Navier-Stokes methods on refined grids. In the present application, the CANARI code is used with the algebraic turbulence model of Michel, Quémart & Durand.

In general, the computation is not made on the complete turbomachine stage. Simplified techniques as the RBC (Reduced Blade Count) or the newly developed PL (Phase-Lagged) techniques are used to limit the dimension and the cost of the computation.

The RBC technique used for 15 years at ONERA on unsteady Euler and Navier-Stokes problems is an original way for treating complete turbomachine stages without changing blade geometry or blade pitches[14][16]. In the newly implemented PL approach, the computation domain is limited to a single blade passage for each row. As the flow is time-periodic in the frame of reference of the rows, the PL technique consists in storing the flow values on the periodic boundaries in order to deal with the phase-lag existing between adjacent blade passages ; similarly, the flow characteristics are stored on the stator-rotor interface boundaries. As the direct storage may lead to very large requirements in CPU memory, the data storage is lowered to a reasonable amount by a Fourier harmonic decomposition. Finally, the periodic boundary condition and the rotor-stator interface are based on the characteristic relations similar to a classical continuity treatment.

Application to the ADTURB turbine stage

The DLR turbine test rig used in the ADTurB BriteEuram Research Project [15] has 43 stator blades and 64 rotor blades. Computations were performed at two operating points corresponding to an expansion ratio of 2.72 (transonic case) and of 1.8 (subsonic case).

The stator grid is made up of 3 structured blocks (H-O-H topology) while the rotor grid includes 4 blocks (H-O-H topology with an H block at the interface). The final grid includes 550293 nodes for one stator blade passage and 597 788 nodes for one rotor blade passage.

In the RBC computation, 2 stator blades and 3 rotor blades are considered which makes about 2.9 10^6 grid points in total. In the PL approach, 1 stator and 1 rotor blades are considered which makes about 1.15 10^6 grid points in total. On the ONERA NEC SX5, computation of one rotor period T_R rotation needs 12000 sec with the RBC technique and about 5000 sec with the PL approach. A preliminary steady flow computation is used to initialize the unsteady computation. In practice, for the RBC computations, at least 12 rotor periods are necessary to reach periodic flow in the transonic case.

The flow interaction between the stator and the rotor includes potential flow effects as seen on the relative Mach number contours (figure 20), but also instantaneous interactions of wakes (seen on the entropy contours at mid-span on figure 20) and shock-waves.

At mid-span on the rotor blade (figure 21), the RBC and PL approaches provide very similar unsteady solutions as the time-averaged and the maximum-minimum envelopes of the static pressure are nearly identical. On the suction side, the static pressure evolution emphasizes high amplitude past the leading edge, while the pressure amplitudes decreases near the trailing edge. Figure 22 shows the first and second harmonic amplitudes of pressure on the rotor blade for the PL calculation. Maximum values of the first harmonic are located on the suction side just downstream of the leading edge with a weaker contribution on the pressure side. In addition, one notices pressure fluctuations in the hub region where secondary flows develop.

In experiment, a Three-Laser-Two-Focus anemometer (3D-L2F) measured the unsteady flow field at mid-span. These test results are compared to the unsteady computation in the stator-rotor gap on figures 24 and 25. These figures show the time evolution of the relative Mach number over two rotor periods (t/T_R) for different reduced azimuthal positions in the rotor system.. The computation presents in general the same time evolution as the experimental data. In the moving frame linked to rotor rotation, one notices the trace of the oblique shock coming from the stator trailing edge and the trace of stator wake which induces low relative velocities (and high relative flow angle).

Figure 23 shows the time-averaged relative flow angle and relative Mach number along the rotor pitch. For both the RBC and PL results, these time-averaged solutions are in close agreement with test with a slight overestimation of the relative Mach number by about $\Delta M=0.03$ and the relative flow angle by about $\Delta\beta=3°$.

For the low pressure ratio test case (subsonic flow), the experimental velocity is also overestimated by about $\Delta M=0.02$ and the relative angle by about $\Delta\beta=3°$. On figure 26, the harmonic analysis of the RBC solution shows on the first harmonic large pressure variations between 25% and 50% of the axial chord on the upper side of the blades, with almost no second harmonic contribution in this case, as it was the case in the transonic case (figure 22).

6. Conclusion

The large influence of unsteady effects in the development of transonic flows around highspeed propeller blades was validated by comparison with test results on an isolated propeller at incidence. In the upwash of a wing and nacelle combination, the complete aircraft Euler computation shows also that unsteady interaction plays a significant role in the transonic flow development around the aircraft wing and nacelle.

On helicopter rotor blades, the natural flow unsteadiness resulting from the combination of rotation and forward flight velocities, is

amplified by the different motions resulting from controls and blade deformations provided by an aeroelastic analysis. The detailed comparison of blade pressure distributions with wind tunnel results validates the present Euler computations on different isolated rotors test cases.

As viscous effects are essential for turbomachinery flows, the 3D unsteady Navier-Stokes computations of rotor-stator interaction requires the use of special techniques as the Reduced Blade Count or the Phase-Lagged technique to take into account the large number of blades. The computed unsteady flow results have been compared favourably with the experimental data available at mid-span of a turbine stage in transonic conditions.

The future applications to be performed with the ONERA *elsA* platform will benefit from synergy and combination of techniques, as the Chimera technique for simplifying mesh construction or new turbulence models for improving Navier-Stokes solutions. This will require validation in term of accuracy and efficiency, with comparison against detailed unsteady measurements on highly instrumented experiments. These developments are essential before routine unsteady computation of complete configurations as an helicopter with main and tail rotor or complete turbo-engine stages, with direct benefits to aeromechanic, aerothermic and aeroacoustic design and optimization.

Acknowledgements

The French Ministries of Defence and Transport, and the European Commission Authorities are acknowledged for their partial funding of the studies presented in this paper.

References

[1] *J.M. Bousquet, P. Gardarein*, Improvements on computations of High Speed Propeller Unsteady Aerodynamics, *ECCOMAS CFD2001 Conference, Swansea, Sept. 2001*

[2] *B. Cantaloube, Ph. Beaumier* Simulation of an unsteady aeroelastic response of a multibladed rotor in forward flight. *27th ERF , Moscow, 2001.*

[3] *G. Billonnet, A. Fourmaux, C. Toussaint,* Evaluation of two competitive approaches for simulating the time-periodic flow in an axial turbine stage, *ETC Conference, Firenze, 2001.*

[4] *A. Lerat, J. Sidès, V. Daru,* An Implicit Finite-Volume Method for Solving the Euler Equations. *Lecture Notes in Physics, Vol. 170, Springer-Verlag, 1982.*

[5] *A.-M. Vuillot, V. Couaillier, N. Liamis,* 3-D turbomachinery Euler and Navier-Stokes calculations with a multidomain cell-centered approach, *AIAA 93-2576, ONERA TP 1993-106*

[6] *N. Liamis , V. Couaillier,* Unsteady Euler and Navier-Stokes Flow Simulations with an Implicit Runge-Kutta Method, *2th European CFD Conference ECCOMAS, Stuttgart , September 5-8, 1994.*

[7] *J.-M. Bousquet*, Theoretical and experimental analysis of high speed propeller aerodynamics, *AIAA 86-1549, ONERA TP1986-64*

[8] *P. Gardarein, J.-M. Bousquet,* ONERA propeller aerodynamic activities in Brite-Euram programmes APIAN-GEMINI, *Workshop on Aerodynamic Engine/Aircraft Integration for Transport Aircraft, 26-27 September 2000, Braunschweig , Germany.*

[9] *M.A. Averardo & al.* Wind Tunnel Tests and CFD Predictions of the Flow-Field of a High-Speed Six-Bladed Propeller in Steady and Unsteady Conditions, *Workshop on Aerodynamic Engine/Aircraft Integration for Transport Aircraft, 26-27 September 2000, Braunschweig , Germany.*

[10] *J. C. Boniface, B. Mialon, J. Sidès,* Numerical Simulation of Unsteady Euler Flow Around Multibladed Rotor in Forward Flight using a Moving Grid Approach. *51st AHS Forum, Fort Worth, 1995.*

[11] *J.C. Boniface, B. Cantaloube, A. Jollès* Rotorcraft simulations using an Object Oriented approach. *26th ERF , The Hague, Sept 26-29,2000.*

[12] *B. Benoit, & al,* HOST, a General Helicopter Simulation Tool for France and Germany, *56th AHS Forum, Virginia Beach (USA), May,2000.*

[13] *G. Servera, P. Beaumier, M. Costes,* A weak coupling method between the dynamic code HOST and the 3D Euler code WAVES, *AST Journal 5-2001.*

[14] *A. Fourmaux,* Assessment of a low storage technique for multi-stage turbomachinery Navier-Stokes computations, *ASME Winter Annual Meeting, Chicago, IL (USA), November 1994.*

[15] *M. Jocker & al,* Parametric Studies of the Aerodynamic Excitation in High Pressure Turbines, *9th International Symposium on Unsteady Aerodynamics, Aeroacoustics, and Aeroelasticity of Turbomachines, Lyon, France, September, 2000.*

[16] *A. Fourmaux, L. Dubois* , Unsteady flow computation in a double-stage double-shaft turbine, *14th ISABE Conference, Firenze (Italy), September 5-9, 1999.*

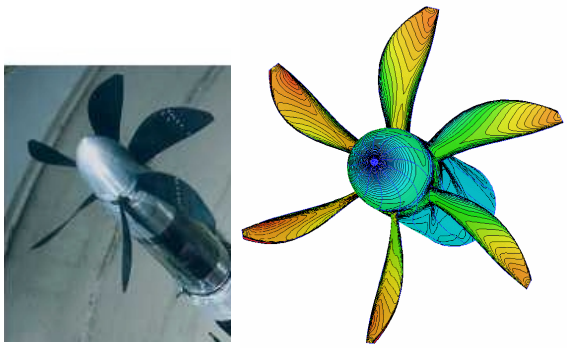

Figure 1 : Isolated APIAN propeller test in S1MA

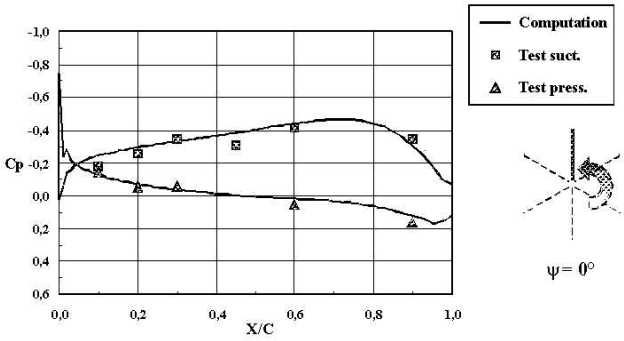

Figure 2a

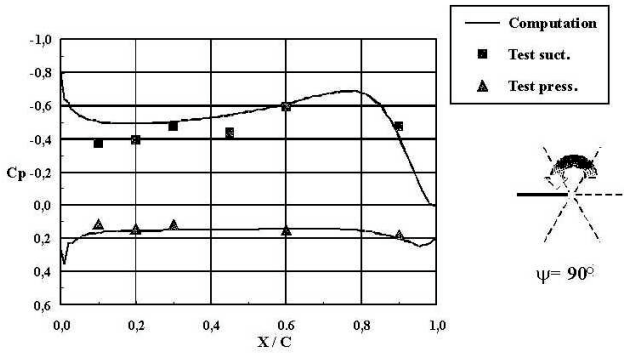

Figure 2b

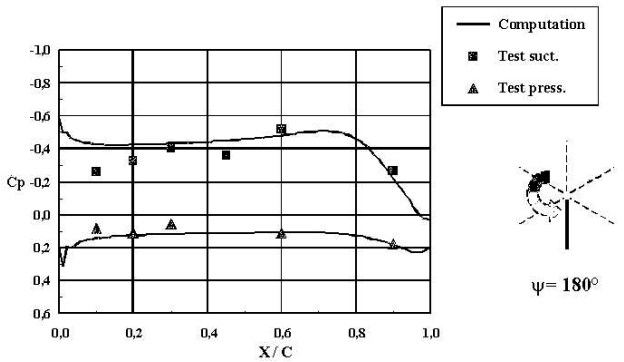

Figure 2c

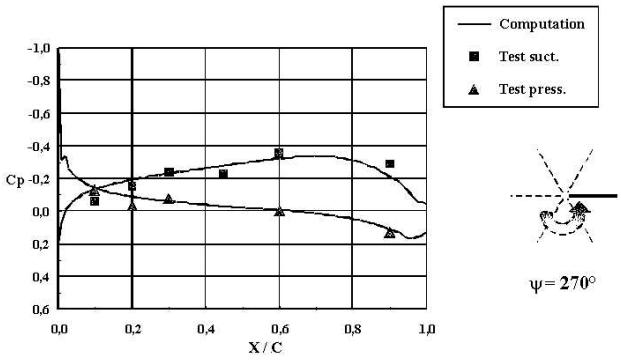

Figure 2d

Figure 2 : Apian propeller blade pressure distribution ; r/R = 0.75. Euler unsteady computation M = 0.7 α = 3° J = 3.12

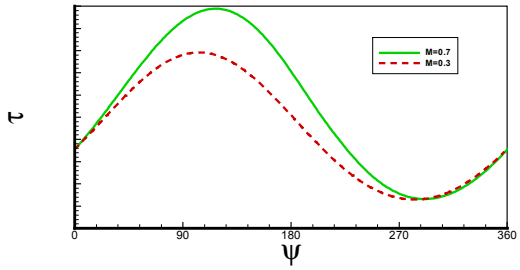

Figure 3 :Blade computed thrust coefficient evolution as function of blade position at M=0.7 and M=0.3.

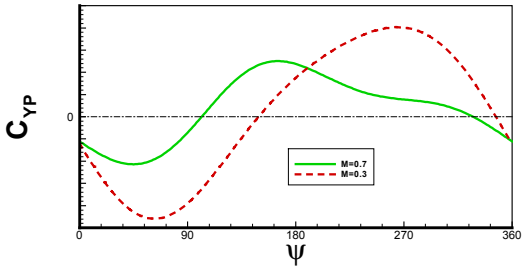

Figure 4 :Blade computed lateral force coefficient evolution as function of blade position at M=0.7 and M=0.3.

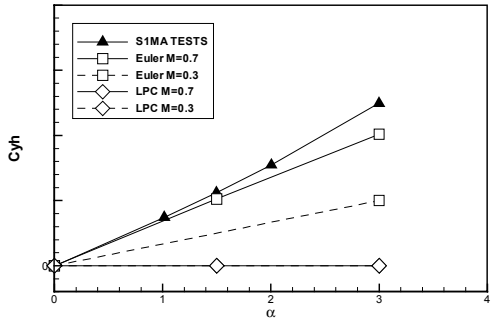

Figure 5: Apian propeller lateral force coefficient. Euler and LPC computation results compared with S1MA experiment.

Figure 6: The half-model of the Generic Transport Aircraft in the S1MA wind tunnel.

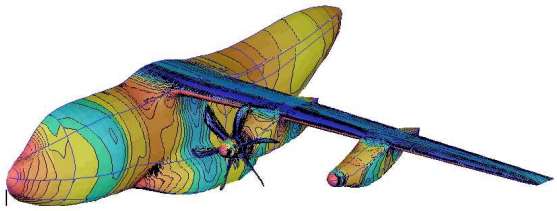

Figure 7: Complete aircraft 3D Euler computation result (half aircraft computed).

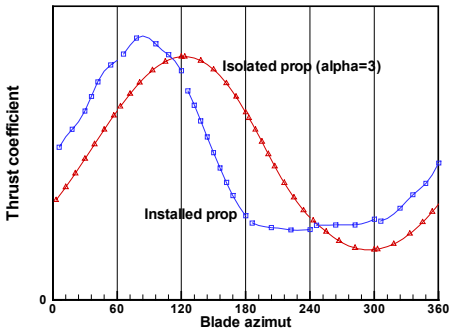

Figure 8: Evolution of computed thrust coefficient on one blade. M=0.68.

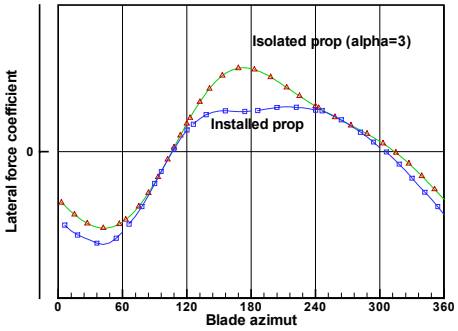

Figure 9: Evolution of computed lateral force coefficient on one blade. M=0.68.

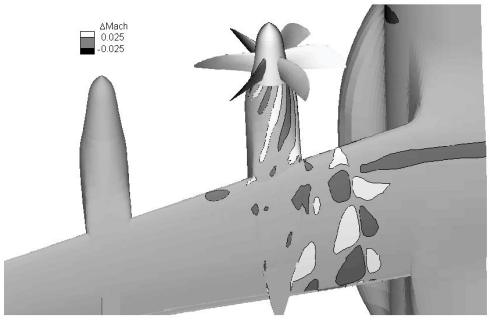

Figure 10: Unsteady interaction effect on wing upper side. (Difference of Mach number distribution between $\psi=0°$ and $\psi=30°$).

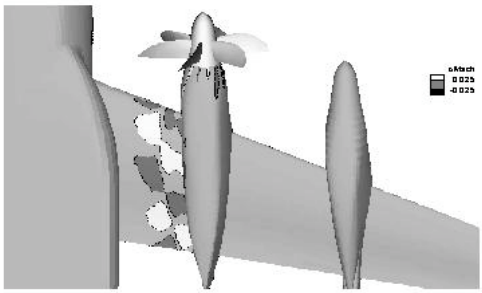

Figure 11 : Unsteady interaction effect on wing lower side. (Difference of Mach number distribution between $\psi=0°$ and $\psi=30°$)

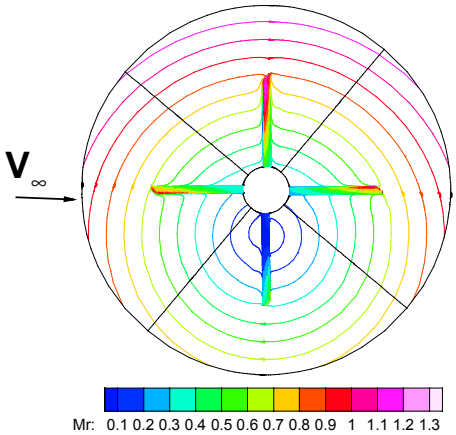

Figure 12: Relative Mach number contours on the 7AD rotor blades in forward flight ($\mu=0.4$)

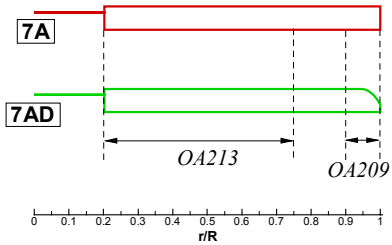

Figure 13 : 7A and 7AD helicopter rotor blades

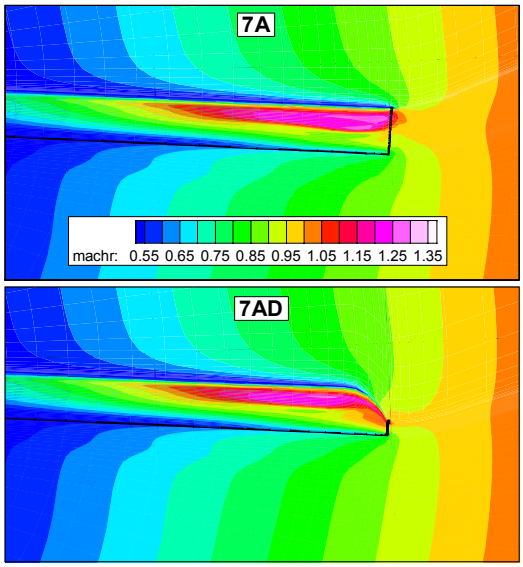

Figure14 : Influence of blade planform on relative Mach number contours (ψ=90°, μ=0.4)

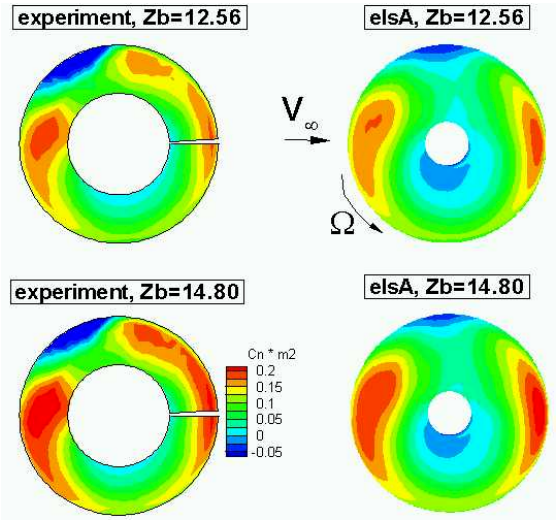

Figure 15 : Influence of rotor lift coefficient on airloads distributions (7A rotor)

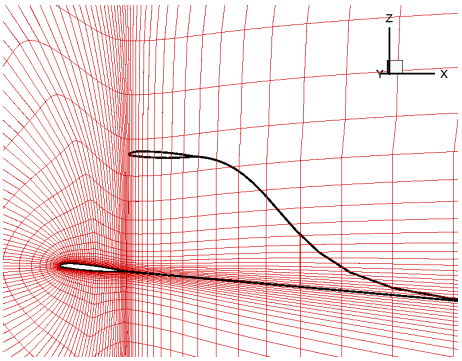

Figure 16: Detail of the 3D grid around 7A blade section near tip (un-deformed blade)

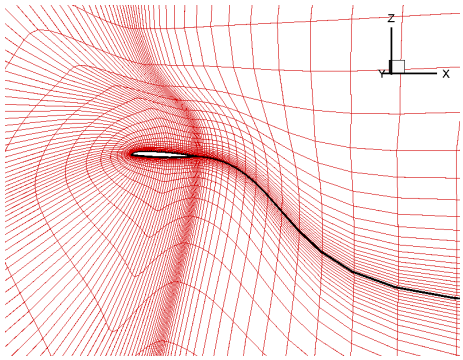

Figure 17: Account of (amplified) blade motion and blade deformation in the 7A blade section grid

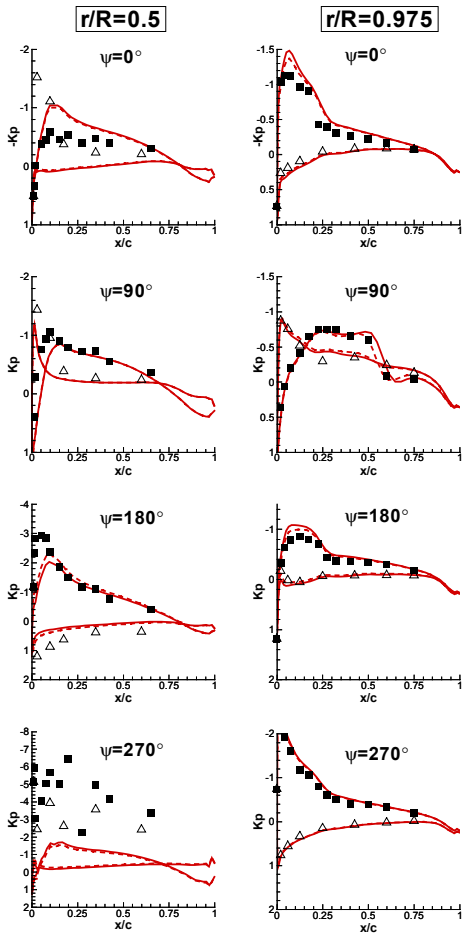

Figure 18 :Influence of 7Arotor blade deformation on pressure distributions (red line=elsA ;black points=exp.)

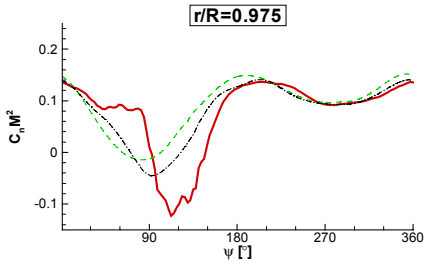

Figure 19 : Influence of blade deformation on 7A rotor unsteady airloads (red line= experiment ; black dotted line =elsA soft blade ; green dotted line=elsA rigid blade)

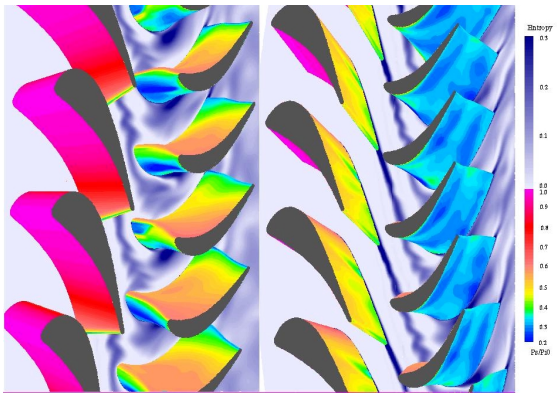

Figure 20: ADTURB turbine stage .3D unsteady Navier Stokes computation of the transonic test case.

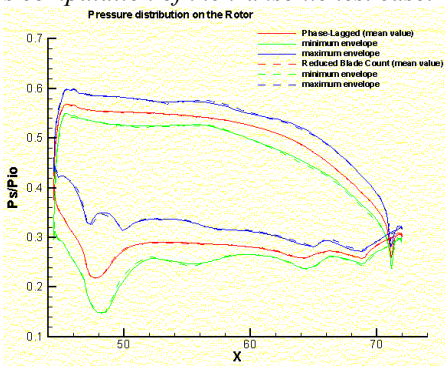

Figure 21:Pressure distribution at midspan on rotor (mini, mean and max level of unsteady pressure evolution on pressure and suction side)

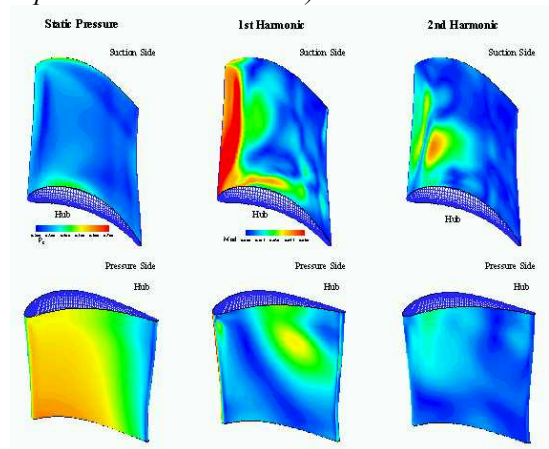

Figure 22 :Fourier analysis of static pressure evolution on the rotor (Phase Lagged computation)

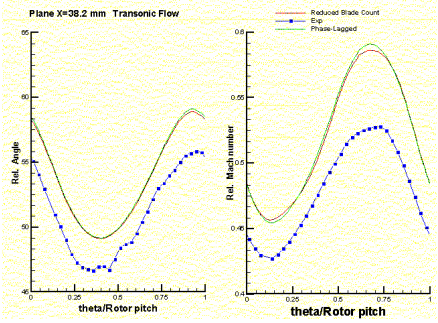

Figure 23: Time-averaged relative Mach number and relative flow angle upstream of the rotor.

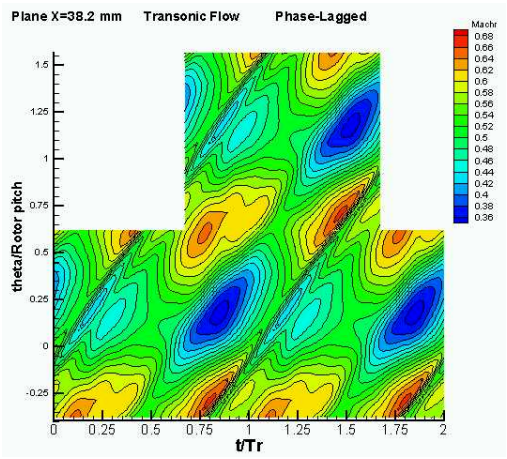

Figure 24:Relative Mach number time-evolution in the plane X=38.2 mm (computation with Phase Lagged approach)

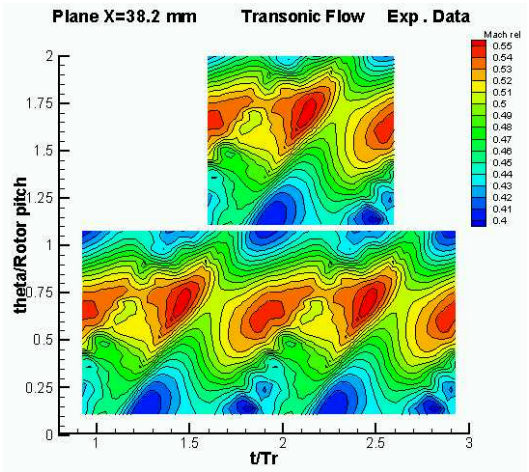

Figure 25: Relative Mach number time-evolution in the plane X=38.2mm (L2F measurement)

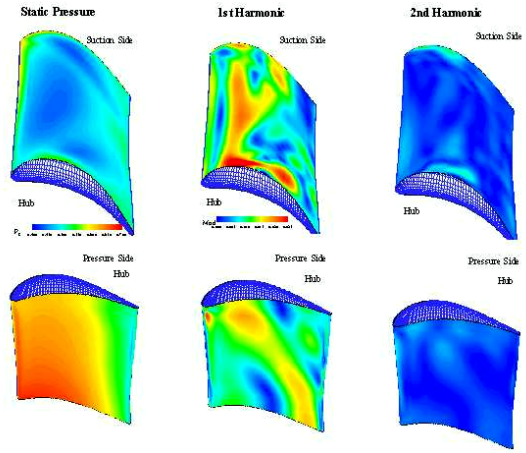

Figure 26 :Fourier analysis of the computed static pressure evolution on the rotor. Subsonic test case flow conditions (Computation with Phase Lagged approach)